Extending Acoustic Liner Bandwidth with Simple Embedded Septa

Brian M. Howerton[1] and Jordan Kreitzman[2]
NASA Langley Research Center, Hampton, VA 23681-2199, USA

Chelsea Solano[3]
Florida State University, Tallahassee, FL 32306, USA

An acoustic liner design incorporating single-hole perforate septa was evaluated by the NASA Langley Liner Physics Team. The design, termed the 'Simplified Septa' concept, incorporates embedded septa as found in traditional, multidegree-of-freedom liners. Generally, such septa are composed of multihole perforates or porous mesh, whereas this concept uses septa with one hole per cell. An optimization scheme was employed to determine septa placement and hole diameters based on a target impedance cost function. Versions of the concept are tested in the NASA Langley Normal Incidence Tube (NIT) to determine impedance and absorption spectra for swept tonal excitation at 120 and 140 dB. Experimental results are compared to predictions from a liner model based on the Zwikker-Kosten Transmission Line (ZKTL) code and show good agreement for no-flow conditions.

I. Nomenclature

L	=	liner cavity depth
d	=	perforate hole diameter
t	=	septa/facesheet thickness
ρ	=	density
c	=	speed of sound
POA	=	percent open area
α	=	absorption coefficient
$\bar{\alpha}$	=	average absorption coefficient
f	=	frequency

II. Introduction

Commercial passenger aircraft must conform to a wide variety of regulations regarding their construction and operation. Many of these regulations are related to safety, but there are also rules on the amount of noise the aircraft can generate. Aircraft engines are the primary contributor to overall noise for much of a flight except for landing where airframe noise tends to dominate [1]. For modern turbofan engines with high bypass ratios, mitigating fan noise with acoustic liners applied to the walls of the inlet and aft bypass ducts has been highly effective in reducing total engine noise [2,3]. Such engines have design features (e.g. fan blade contouring, blade lean/sweep, etc.) which lead to reduced source levels at the blade passage frequency (BPF) and its harmonics relative to the broadband noise components of the total noise spectrum [4]. As fan diameters increase, their rotation speeds have been reduced to prevent shock-associated noise at the blade tips which effectively shifts the noise spectra to lower frequencies. Nacelles are also trending toward more compact designs to reduce drag and save weight which puts a premium on

[1] Research Scientist, Applied Acoustics Branch, Senior Member AIAA, (brian.m.howerton@nasa.gov).
[2] Research Scientist, Applied Acoustics Branch, Member AIAA, (jordan.r.kreitzman@nasa.gov).
[3] Intern, Department of Mechanical Engineering, Member AIAA, (cad12e@fsu.edu).

acoustic liner efficiency to make up for the loss of treatment area. Taken together, these design paradigms motivate the consideration and development of liner concepts with wider absorption bandwidth.

Figure 1 shows examples of liners typically used in aircraft engines. The single-degree-of-freedom (SDOF) liner can be tuned through changes in core depth and facesheet geometry to provide excellent absorption for a narrow range of frequencies (approximately one octave). Widening the frequency range of effective absorption can be accomplished by embedding a porous septum within the liner core to create a two-degree-of-freedom (2DOF) liner. The additional resonant frequencies extend the effective frequency range to two octaves. Further benefit could be gained by incorporating additional septa, but this must be weighed against the additional complexity and cost. Advances in manufacturing may offer future opportunities to take advantage of these multisepta concepts.

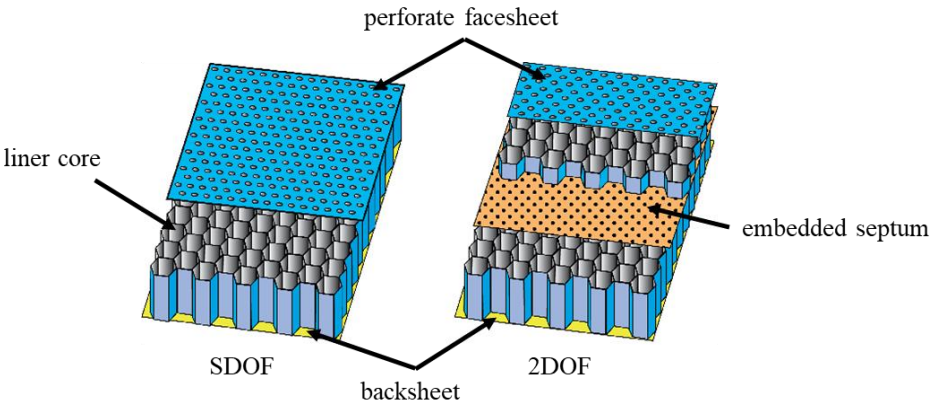

Fig. 1 Conventional liner construction

This paper details the design and evaluation of two sets of acoustic liners incorporating the Simplified Septa (SS) concept whereby multiple embedded septa in each cell of the liner core, each with a single perforation, are used to improve broadband liner absorption. An optimization scheme targeting absorption performance over a frequency range of 400–3000 Hz is employed to design the initial set. Samples for this set are constructed using additive manufacturing. A second set is made with state-of-the-art techniques and materials for flightworthy liners where the pertinent septa details (hole size and depths) are duplicated. These samples are tested in the NASA Langley Normal Incidence Tube using swept-sine tonal excitation at sound pressure levels (SPLs) of 120 and 140 dB. Normalized specific acoustic impedance (hereafter referred to as impedance) spectra educed from this testing are compared to predictions from a liner impedance model.

III. Background

A. Simplified Septa Concept

Earlier work has shown that using embedded perforate septa can extend the absorption bandwidth of acoustic liners by creating a double-Helmholtz resonator system with multiple resonances [5,6]. Septa materials range from traditional perforates, similar to typical facesheets, to microperforates and meshes. Tuning for a specific impedance spectrum is accomplished by varying septum porosity, thickness and placement within the core. The Simplified Septa concept is an alternative embodiment of this type of liner that may be attractive for some applications. The intent of this concept is multi-faceted. By constraining septum porosity to a single hole, there can be potential manufacturing benefits when building the liner core. Depending on hole size, the perforation can potentially be punched, drilled or lasered either before or after septum placement. Such a design is also suitable for construction via additive manufacturing as the perforations are more likely large enough to be within the limits of such methods. The use of a single hole generates dissipation through the creation of vortical structures separating from the hole edges especially at high SPLs. As these acoustically-generated structures decay, their energy is converted to heat. Thus, the liner is expected to be nonlinear with increasing acoustic levels. Furthermore, the concept has potential for better low frequency absorption due to the larger holes employed. These would result in larger end correction values, since the correction is based on diameter, and should make the liner perform as if it were deeper [7].

The concept is similar to a liner developed by Ross et al. [8] that also used single-perforate embedded septa but with some key differences. For SS, the liner is constructed from an array of identical unit cells, each with multiple embedded septa, to achieve broadband performance while Ross uses a single septum per cell at varying cell depths.

Their arrangement is more akin to a multidegree-of-freedom (MDOF) liner as described by Sutliff et al. [9]. Each unit cell of SS is intended to be identical, giving a uniform impedance, yet still providing absorption over a wide frequency range.

B. Septa Optimization

Septa placement, hole sizing and facesheet parameters were determined using an optimization tool that incorporates a liner model derived from theory used in the NASA Zwikker and Kosten Transmission Line (ZKTL) impedance prediction code [10-13]. In this code, the acoustic pressures and particle velocities are calculated by stepping through the acoustic liner from the backplate to the liner surface. This optimization task was performed using the "fmincon" function in MATLAB as it can provide solutions for constrained nonlinear problems involving multiple variables [14]. Among the various algorithms available in "fmincon", sequential quadratic programming (SQP) is utilized for its efficiency and ability to maintain bounds throughout iterations. The solver may converge to a local minimum rather than the global minimum given the complexity of the variables involved. To mitigate this, a basin hopping routine is incorporated into the solver. Furthermore, the initial guess is diversified to explore the solution space and increase the likelihood of finding the global solution.

Constraints were placed on the optimizer to limit certain geometric features of the liner to enable construction via additive manufacturing with the stereolithography process. Figure 2 gives a diagram of a unit cell with pertinent dimension labels. Table 1 summarizes the bounds on those geometric features. Perforate hole size was limited to a minimum diameter of 0.51 mm and a maximum of 2.54 mm. Spacing between septa was also constrained to values between 4.57 mm and 15.24 mm. Reflecting practical experience in liner design and applications on real-world engines, total liner thickness was limited to a maximum of 50.8 mm. The number of septa for a design was specified as a fixed parameter for the optimizations.

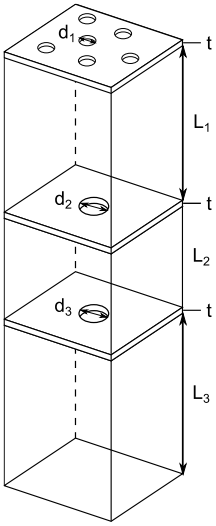

Fig. 2 AM Liner core unit cell diagram.

Table 1. Simplified Septa liner optimization constraints.

	Description	Lower Bound	Upper Bound
Facesheet and Septa	hole dia. (d_n)	0.51 mm	2.54 mm
	thickness (t)	0.51 mm	2.54 mm
	POA	4 %	16 %
Cavities	total length (L)	0.81 mm	50.8 mm
	L_n	4.57 mm	15.24 mm

There are many potential objective functions that can be employed to optimize liner impedance depending on the design goal. With the goal of improving broadband absorption, the selected objective was to maximize the absorption coefficient over a targeted frequency range. The design variables are contained in a vector X:

$$X = [d_1, d_2, \ldots d_n, t, POA, b, L_1, L_2, \ldots L_n] \quad (1)$$

To maximize the average absorption coefficient within a minimization framework, the negative of this quantity over a specified frequency range is used, as given by:

$$\bar{\alpha} = \frac{1}{f_2 - f_1} \int_{f_1}^{f_2} \alpha(X) df \quad (2)$$

Where X is the vector of constrained design variables to be optimized, f_1 was the lowest and f_2 was the highest frequency of interest. For the current study, these frequencies were set to 600 and 3000 Hz, respectively, to reflect the majority of the testing range. A source SPL of 120 dB was chosen for this optimization.

IV. Experiment

The experimental investigation involves two phases of testing. The first evaluates additively manufactured samples consisting of the liner core and a separable facesheet fabricated using a stereolithography process whereby liquid plastic resin is photopolymerized to build the part. A second phase looks at samples using the same perforate diameters and septa depths but applied to a phenolic honeycomb core manufactured in collaboration with Hexcel Corporation. Again, a separate facesheet is used with these core designs. These samples are used to evaluate the concept in an embodiment employing state-of-the-art manufacturing techniques already certified for flight.

A. Liner Core Construction

The additively-manufactured (AM) liners for the NIT use a 5x5 grid of 7.62 mm square unit cells separated by 2.54 mm partitions to form an active area of 2581 mm^2. This active area matches the cross-section area of the NIT. Table 1 provides the dimensions for the two Phase 1 core samples, the first with two embedded septa (AM2S) and the second with three embedded septa (AM3S).

Images of the AM3S core are provided in Fig. 3 showing the uppermost embedded septum with the single perforation per cell and a side view of the same core where the three embedded septa are visible through the sample sidewall. Note that the septa thickness is constant for all samples at 0.81 mm. Both samples are made with the same Accura 60 resin from 3D Systems. When mounted in the NIT, the cores are clamped in place by a 25.4 mm thick brass plate that serves as a backsheet to the unit cells.

Table 2. Liner core unit cell dimensions.

Dimension (mm)	2 Septa (AM2S)	3 Septa (AM3S)
t	0.81	
d_1	0.81	
L_1	14.40	10.8
d_2	1.07	2.00
L_2	10.49	10.8
d_3	0.64	0.81
L_3	7.52	10.8
d_4	N/A	0.81
L_4	N/A	10.8
Total Length	34.03	45.62

Samples for Phase 2 testing are made from commercially available phenolic honeycomb (PH) core using state-of-the-art manufacturing techniques. These samples have perforate diameters, septa placements and core lengths identical to the AM cores but differ in several parameters. Cell size is 9.53 mm flat-to-flat with a much smaller partition thickness at 0.5 mm. Septa thickness is also reduced to 0.25 mm owing to the PEEK plastic film used to create them. The cores are bonded to a 6.35 mm thick aluminum backing plate and pressed into an aluminum sleeve serving as the sample holder. The holder has a square inner shape 50.8 mm in width and outer dimensions that match the AM cores. Figure 4 provides images of the two PH core samples with the embedded septa and their perforations visible along the core edge.

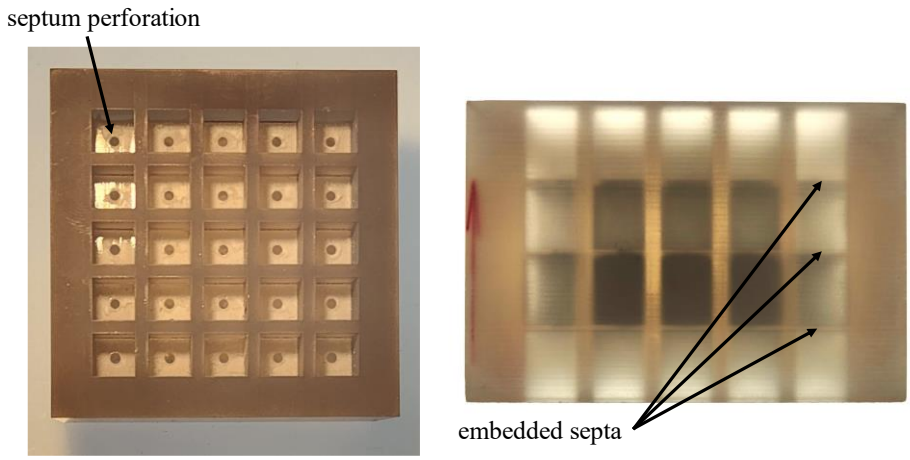

a) Top view **b) Side view**

Fig. 3 Example of an additively manufactured Simplified Septa liner core (AM3S) [Photo Source: NASA].

a) PH2S **b) PH3S**

Fig. 4 Phenolic honeycomb core samples [Photo Source: NASA].

B. Liner Facesheet Construction

A common facesheet is used for both AM samples incorporating six perforations per cell distributed as shown in Fig. 2. The facesheet is 0.81 mm thick with round perforations of the same diameter (t/d = 1). This geometry results in a percent open area (POA) of 3%. Overall dimensions are 63.5 mm square to match the sample core. Figure 5 is an image of the facesheet, which is made from the same Accura 60 resin as the core samples. The PH core samples had a fine wire mesh facesheet with a resistance of 27 cgs Rayls.

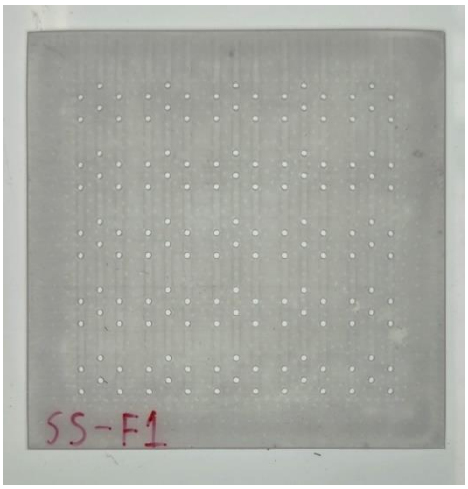

Fig. 5 AM liner sample common facesheet [Photo Source: NASA].

C. Normal Incidence Tube

The Normal Incidence Tube (NIT) consists of a group of six electromagnetic acoustic drivers coupled radially into a cylindrical tube that transitions to the 50.8 mm x 50.8 mm square cross-section waveguide. Samples are placed at the exit of the tube to be exposed to the generated sound field. Individual digital-to-analog converters for each speaker allow for the creation of arbitrary waveforms to energize each driver. Typically, tonal or broadband signals are employed for impedance eduction. For tones, levels of 150 dB can be consistently achieved while broadband is limited to an overall SPL of 140 dB across the typical measurement range of frequencies (400–3000 Hz). Impedance spectra for each sample are obtained in the NIT via the switching Two-Microphone Method (TMM) [16]. The key feature of the TMM is the efficient acquisition of the complex transfer function spectra between two flush-mounted microphones strategically located in the standing wave field from which the complex reflection factor is calculated. Transfer function accuracy is assured by a microphone switching technique that avoids labor intensive amplitude and phase calibrations. Several operational features have also been incorporated to maximize test efficiency. The microphone switching is automated by means of a computer-controlled stepping motor that rotates the microphone holder while a feedback loop and iterative scheme is used to adjust sound pressure levels to the desired value. Custom software controls all aspects of the acquisition and reporting process and can step through a test matrix without user intervention. Figure 6 shows the general arrangement of the NIT apparatus.

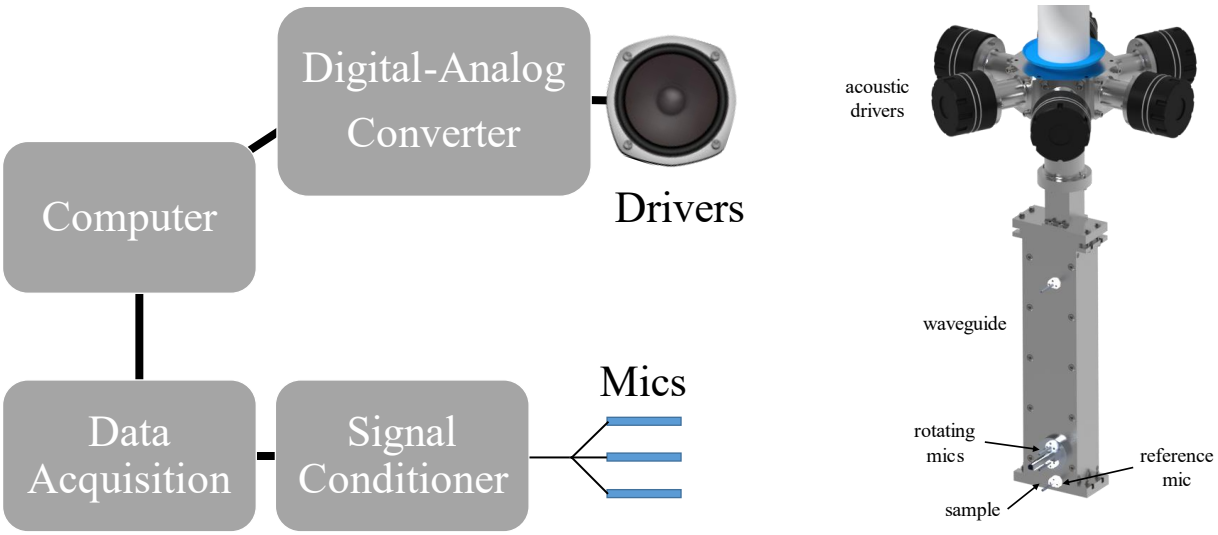

Fig. 6 NASA Langley Normal Incidence Tube general arrangement.

D. Measurement Process

The Swept-Sine Method (SSM) [15] is used to obtain the complex acoustic cross spectra between the measurement microphones and the source signal supplied to the acoustic drivers. The method offers increased frequency resolution and reduced data acquisition time by sweeping sinusoidal excitation continuously across the frequency range instead of sequentially dwelling on discrete frequencies as in a stepped-sine process. The acoustic source signal linearly increases in frequency during the measurement process and is amplitude modulated to provide a constant desired total SPL at the sample surface. A Vold-Kalman order tracking filter is employed to extract complex acoustic pressures at each microphone for the frequencies of interest. The sweep is played back for each microphone orientation of the TMM with the resulting SPL and phase data processed using the Multipoint Method of Jones and Stiede [16].

V. Results and Discussion

A. Phase 1 - Additively Manufactured Samples

Impedance and absorption spectra from NIT testing as well as corresponding predictions using ZKTL are shown for the AM2S sample in Figs. 7 and 8. Acoustic excitation levels of 120 dB (Fig. 7) and 140 dB (Fig. 8) were used. The solid lines represent the test data ('Exp.' in the legend) while the dashed curves are the model predictions ('Model' in the legend). Initial comparisons of the model to experimental results (not shown here) revealed significant differences for the higher SPL due to nonlinear effects not included in the original formulation. Modifications to the standard ZKTL code were made to incorporate a new perforate model, as developed by Kreitzman and Jones [17], that includes nonlinear resistance due to acoustic particle velocity effects as well as radiation reactance. Results from this updated model are shown.

For 120 dB excitation, the two-septa geometry has an impedance spectrum with three resonances in the test frequency range as seen from the reactance plot. Values for reactance are generally between -4 and 1 except at the lowest frequencies. Resistance is less than 2 for much of the frequency range but rises above that level in the areas of antiresonance. Such resistance peaks are frequently observed in perforates with larger hole diameters or at lower SPLs. Absorption coefficients are greater than 0.5 for most of the frequency range. Liners with normal incidence absorption coefficients above 0.4 have, historically, provided significant attenuation when evaluated in a grazing incidence environment. It is therefore assumed that this sample is exhibiting good broadband absorption characteristics over a wide frequency range. Overall, good agreement between experimental data and impedance model predictions is obtained over much of the frequency range. Some overprediction of resistance and an upward frequency shift is observed for the second antiresonance. Reactance is captured fairly well but exhibits the same frequency shift as the resistance plot for the second antiresonance.

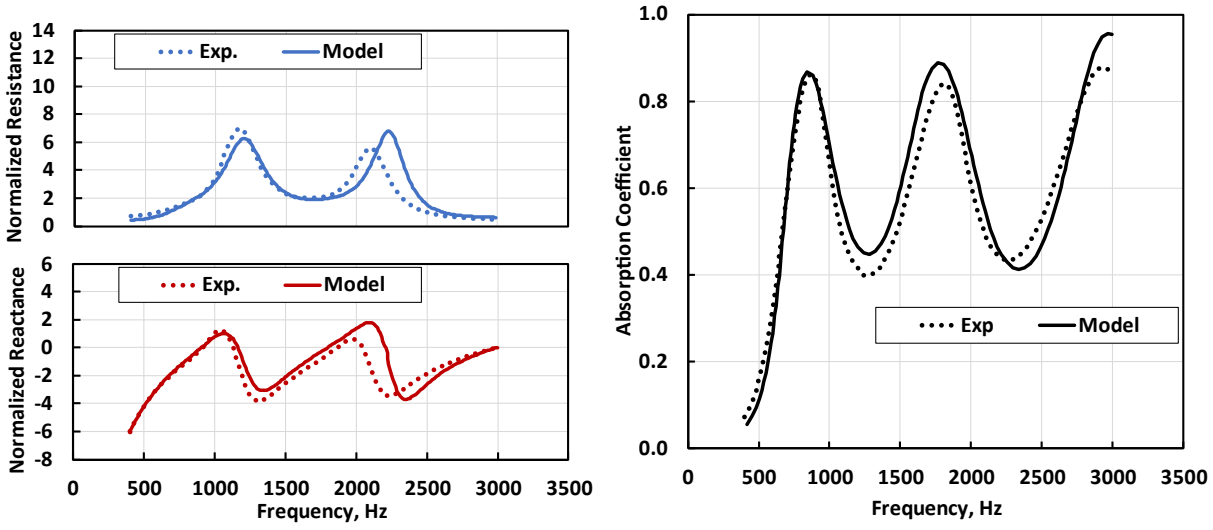

a) Impedance **b) Absorption**

Fig. 7 Experimental impedance and absorption spectra compared to liner model predictions for Sample AM2S, 120dB total SPL.

Increasing the excitation SPL to 140 dB (Fig. 8) results in significantly different impedance spectra. The antiresonances seen earlier are no longer apparent with reactance flattening and taking on a more -cot(*kL*) type

behavior. Peak resistances are reduced, but values are generally higher away from the antiresonances. The absorption coefficient in Fig. (8b) steadily increases with increasing frequency as resistance approaches unity and the reactance approaches zero. As the design optimization was done for 120 dB excitation, it is understandable that performance at 140 dB could be reduced but useful absorption is still occurring from approximately 900 Hz and above. The model captures the variation in reactance and the overall trends quite well but slightly overpredicts resistance in the mid and upper frequencies.

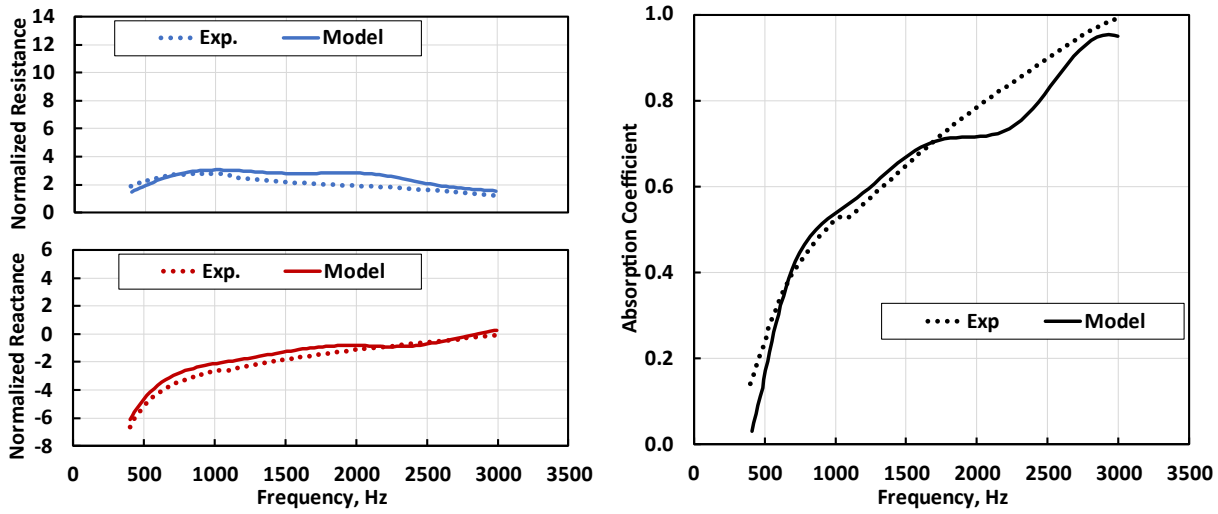

a) Impedance **b) Absorption**

Fig. 8 Experimental impedance and absorption spectra compared to liner model predictions for Sample AM2S, 140dB total SPL.

Comparisons of the experimental results and liner model for the AM3S sample are provided in Figs. 9 and 10 for the two sound pressure levels. In Fig. 9 for 120 dB SPL, the increase in core depth, relative to the AM2S sample, lowered the first resonant frequency from ~900 Hz to ~750 Hz. Resistance stays between 1 and 2 for most of the frequency range tested except near the antiresonance observed at 1000 Hz. Including a third septum in this configuration does not seem to result in an additional resonance in the test frequency range. Good absorption values are seen in two frequency bands between 500–800 Hz and 1500–2600 Hz. Good agreement is obtained between liner model predictions and experimental results for all frequencies.

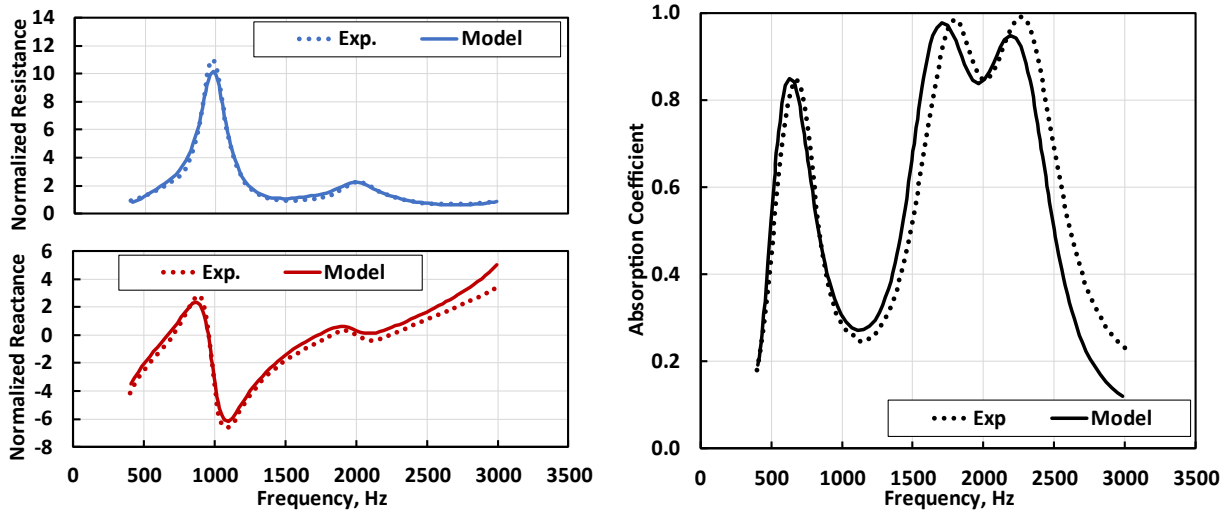

a) Impedance **b) Absorption**

Fig. 9 Experimental impedance and absorption spectra compared to liner model predictions for Sample AM3S, 120dB total SPL.

Increasing excitation SPL to 140 dB produces the results shown in Fig. 10. Impedance trends are similar to those observed for AM2S at the same source levels where resistance peaks at the lower frequencies then decreases. Reactance increases almost linearly but crosses zero at a much lower frequency resulting in peak absorption at 1900 Hz rather than 3000 Hz for AM2S. The impedance model generally performs well with accurate predictions of resistance and reactance and a good capture of the absorption trend.

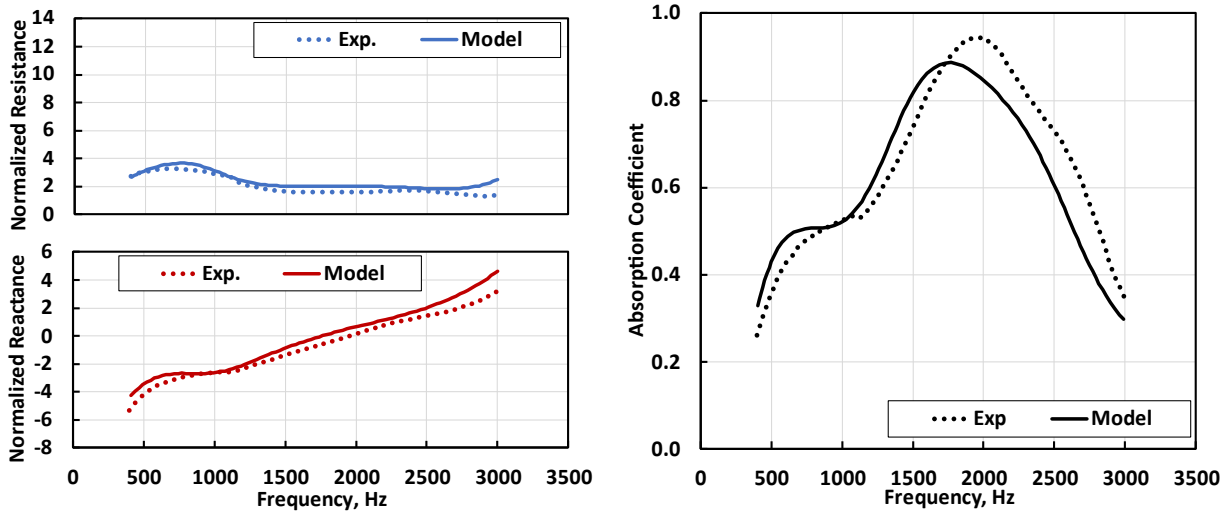

a) Impedance **b) Absorption**

Fig. 10 Experimental impedance and absorption spectra compared to liner model predictions for Sample AM3S, 140dB total SPL.

The impedance variation with SPL confirms the expected nonlinear behavior of the SS design. The core from AM2S was retested with a 27 cgs Rayl wire mesh facesheet as an attempt to isolate the nonlinear effects of septa from the facesheet. Figure 11 plots measured acoustic impedance and absorption coefficient spectra for a range of total sound pressure levels from 100 to 140 dB. Each quantity shows significantly reduced frequency variation with increasing SPL. As the mesh facesheet has very linear characteristics with SPL, the variation shown appears to be driven by the core, and hence, the septum geometry. Absorption is negatively affected by this choice of facesheet as it appears to have increased resistance above optimum. If the geometry of the facesheet is included in the design optimization such that the facesheet resistance could be reduced, better performance may be achieved. Reactance values are also shifted downward likely due to the loss of mass reactance.

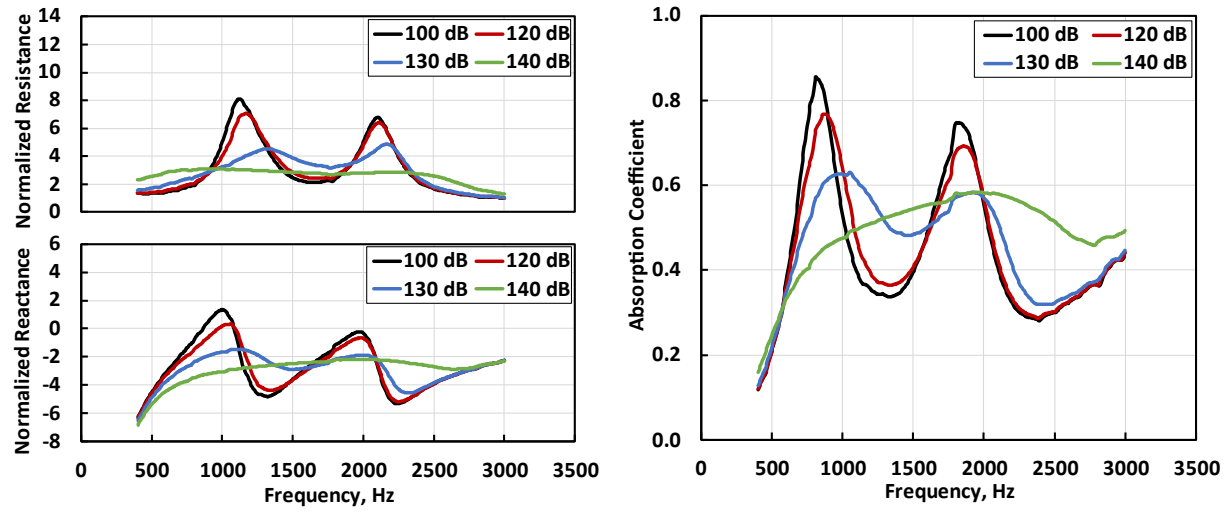

a) Impedance **b) Absorption**

Fig. 11 Experimental impedance and absorption spectra for Sample AM2S core with 27 CGS Rayl mesh facesheet.

B. Phase 2 - Phenolic Honeycomb Samples

NIT experimental results compared with model predictions for the second set of liner samples using the phenolic honeycomb cores with a 27 cgs Rayl mesh facesheet are shown in the figures below. Given the differences noted earlier in partition/septa thickness and the facesheet used, one should not expect identical behavior with the earlier AM results even though the septa designs and placements are similar. Rather, the intent of this set was to verify that the method of construction did not fundamentally change the performance of the concept such that broadband absorption was no longer observed.

Impedance results for PH2S are provided in Figs. 12 and 13 for excitation at 120 and 140 dB SPL. Experimentally, resistance tends to increase over the frequency range for the 120 dB case while results for 140 dB are relatively flat. The model performs reasonably well predicting resistance at both SPL's except for frequencies between 1100 to 1750 Hz at 120 dB. In that region, the experimental data has resistance remaining near constant at 2 whereas the model

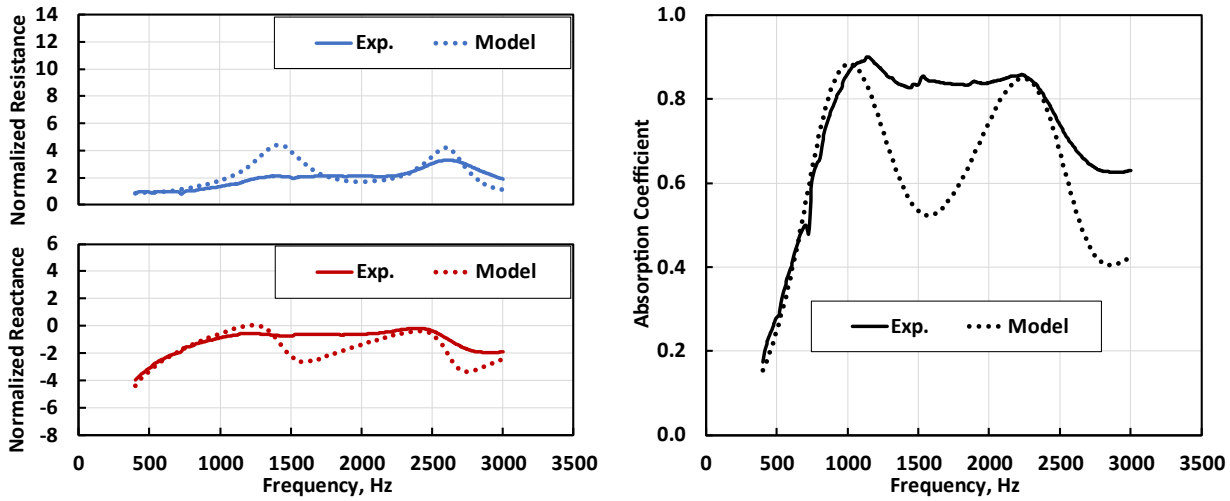

a) Impedance **b) Absorption**

Fig. 12 Sample PH2S experimental acoustic impedance spectra compared to ZKTL liner model results, 120 dB total SPL.

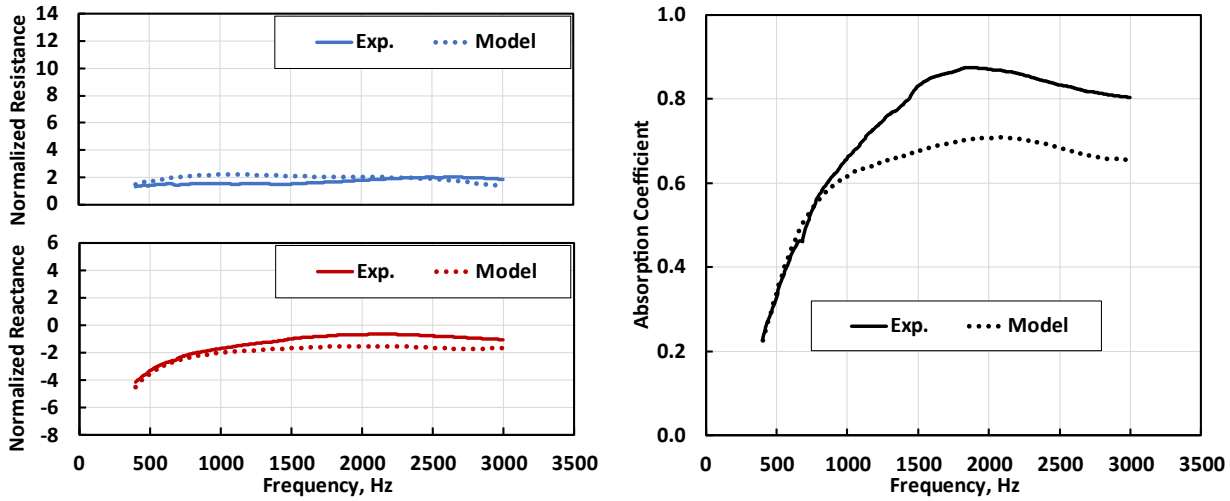

a) Impedance **b) Absorption**

Fig. 13 Sample PH2S experimental acoustic impedance spectra compared to ZKTL liner model results, 140 dB total SPL.

predicts an antiresonance peak at 1400 Hz not seen in the test data. Behavior, however, of a second antiresonance at 2600 Hz is captured more accurately. For reactance at 120 dB, simulation shows even greater variation in values that is not matched by the experimental data at the middle and upper frequencies. Increasing excitation to 140 dB eliminates

this variation with the model capturing the calculated reactance quite well. Absorption coefficients determined from the test data are above 0.5 starting at 700 Hz and remain higher up to 3000 Hz as shown. Given that optimal resistance for normal incidence is 1, using a lower resistance facesheet may further improve absorption performance. The aforementioned differences between experimental and modeled impedance spectra result in significant variance in absorption coefficient curves at both SPL's. Agreement is good up to 1000 Hz, but the predicted dips for 120 dB, centered at 1500 and 2700 Hz, and the general underprediction for 140 dB are not matched experimentally.

Measured and predicted impedance spectra at 120 and 140 dB for PH3S (Fig. 14 and 15, respectively) show resistance and reactance trends similar to those for PH2S. Variability was, again, reduced with increasing SPL and reactance was generally less than zero across the frequency range. Nominal values for both resistance and reactance were similar for both excitation levels. This contrasts with the AM samples from Phase 1 where the differences in spectra were much more pronounced for the two source SPL's. The added core depth of PH3S improved low frequency absorption, with meaningful attenuation beginning approximately 200 Hz lower than observed for the PH2S sample (500 vs 700 Hz). As with PH2S, the liner impedance model does not capture the midfrequency portion of both the resistance and reactance spectra at 120 dB but gives good agreement elsewhere. The comparison at 140 dB is

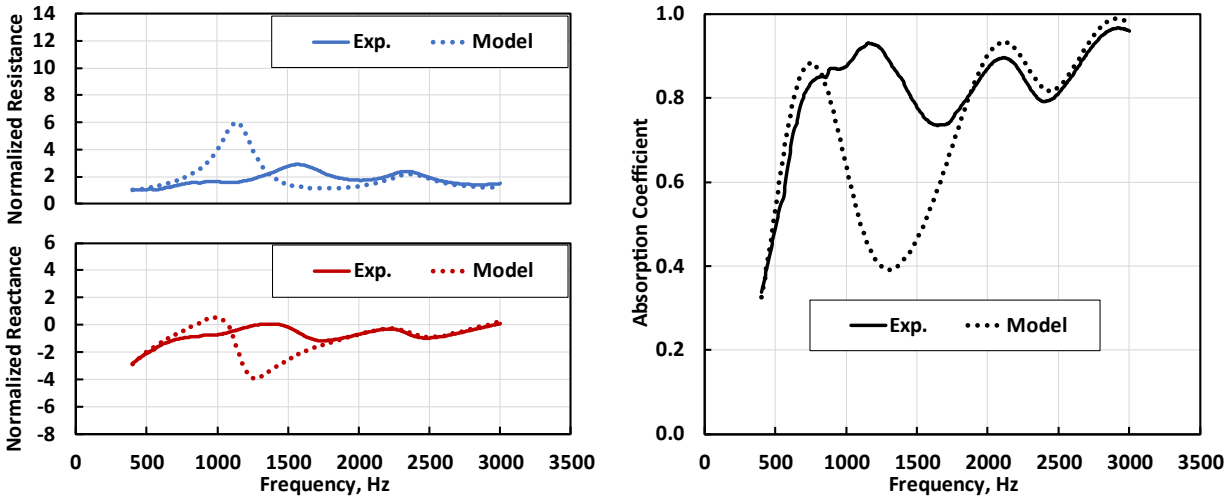

a) Impedance **b) Absorption**

Fig. 14 Sample PH3S experimental acoustic impedance spectra compared to ZKTL liner model results, 120 dB total SPL.

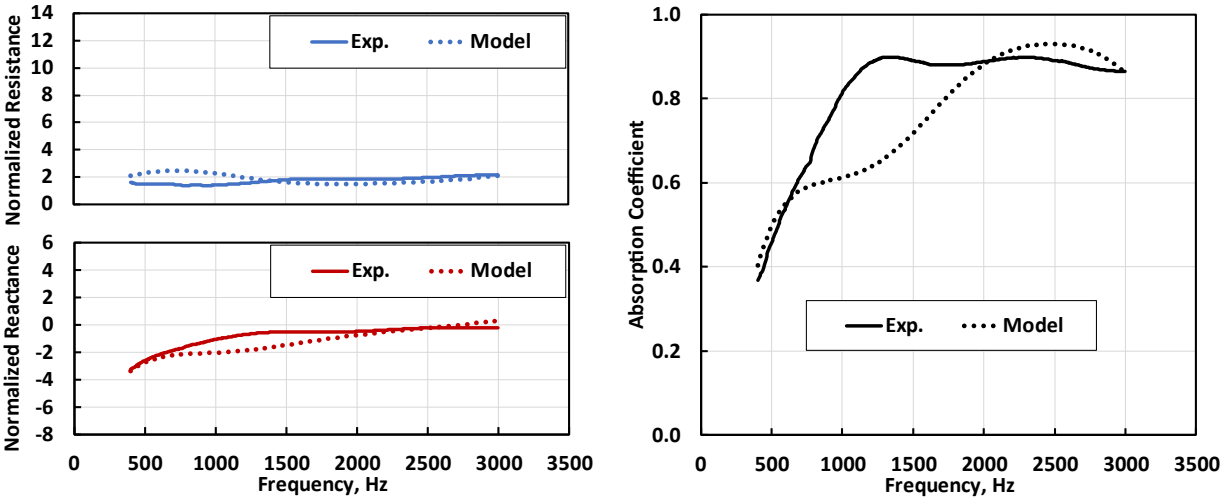

a) Impedance **b) Absorption**

Fig. 15 Sample PH3S experimental acoustic impedance spectra compared to ZKTL liner model results, 140 dB total SPL.

improved, however, as the spectra are rather invariant in their impedance values. Some deviation is observed in the reactance results from 750 to 1800 Hz with corresponding deviation in the absorption coefficient.

There are several possibilities to explain why the model works reasonably well for the AM samples but is less predictive for the PH configurations. The AM samples have a very regular and consistent geometry with an integer number of cells whereas the PH samples have a number of partial cells along the perimeter (see earlier photos) with variable porosity depending on how the sample was cut. These effects can be modeled with additional complexity but are unique to each sample and not representative of the intended cell design. One could fill those partial cells with a rigid material to eliminate their effect which should improve the modeling of the remaining full cells. Furthermore, the embedded septa are not entirely rigid, as assumed in the model. A sample with unperforated septa could be built and tested to determine those compliance parameters. Properly accounting for the PH core blockage, which should be a small percentage of the total sample area, is also warranted. The unmodeled liner aspects, in aggregate, appear to benefit overall performance. Understanding these aspects could be useful in improving future designs.

In general, both PH configurations produced very good absorption over a wide frequency range as desired. Based on the results, however, some improvement could still be obtained by adjusting the resistance closer to the optimal ρc value. The variation in impedance with SPL implies nonlinear behavior by the sample, as hypothesized earlier. In this case, the use of a linear mesh facesheet suggests that the core, and hence, the septa, are responsible for this nonlinearity.

VI. Conclusions

The Simplified Septa liner concept was developed and evaluated for its acoustic performance. Two- and three-septa configurations were made using both additive manufacturing (AM) and a phenolic honeycomb (PH) construction techniques. Experimental testing in the NIT at multiple sound pressure levels showed promising impedance and absorption characteristics with good broadband performance. Impedance behavior and absorption performance varied with SPL as expected although the PH samples seem less affected by excitation SPL. Modeling of these configurations using a version of ZKTL with terms to account for nonlinear acoustics agreed well with the measured data for the AM samples. Comparisons were not quite as good for the PH configurations likely due to several factors not included in the model. Those factors will be incorporated into a revised model suitable for use in design optimizations of this concept.

Acknowledgments

The authors would like to thank Robert Andrews from the NASA Langley Additive Manufacturing Facility and Clark Smith of Hexcel Corporation for their efforts in fabricating test samples. This work was conducted in support of the NASA Advanced Air Transport Technology Project for the Advanced Air Vehicles Program.

References

[1] Van Zante, D, Nark, D. M., Fernandez, H., "Propulsion Noise Reduction Research in the NASA Advanced Air Transport Technology Project," *International Society for Air Breathing Engines 2017,* Manchester, UK, Sept 2017.

[2] "The NASA Acoustically Treated Nacelle Program," *Proceedings of the Aircraft Noise Symposium* (Acoustical Duct Treatments for Aircraft), Invited Tutorial Papers presented at the *77th Meeting of the Acoustical Society of America*, Philadelphia, PA, Apr. 1969.

[3] "Study and Development of Turbofan Nacelle Modifications to Minimize Fan-Compressor Noise Radiation," Vol. IV – Flight-worthy Nacelle Development, Prepared by The Boeing Company, NASA CR-1714, Jan. 1971.

[4] Bielak, G. W., Premo, J. W., and Hersh, A. S., "Advanced Turbofan Duct Liner Concepts," NASA CR-1999-209002, February 1999.

[5] Gautam, A., Celik, A., and Azarpeyvand, M., "Double Degree of Freedom Helmholtz Resonator Based Acoustic Liners," AIAA Paper 2021-2205, August 2021.

[6] Lee, F. C., Chen, W. H., "Acoustic Transmission Analysis of Multi-Layer Absorbers," *Journal of Sound and Vibration*, Vol 248, No. 4, 2001, pp. 621-634.
doi:10.1006/jsvi.2001.3825

[7] Ingard, U., "On the Theory and Design of Acoustic Resonators," *The Journal of the Acoustical Society of America*, Vol. 25, No. 6, 1953, pp. 1037–1061.

[8] Ross, E. P., Bennett, G. J., Figueroa-Ibrahim, K. M., Morris, S. C. and Sutliff, D. L., "Evaluation of an Additively-Manufactured Acoustic Metamaterial as a Nacelle Liner using the Advanced Noise Control Fan," AIAA Paper 2023-3827, June 2023.

[9] Sutliff, D. L., Nark, D. M., and Jones, M. G., "Multi-degree-of-freedom Liner Development: Concept to Flight Test," *International Journal of Aeroacoustics*, Vol. 20(5-7), 2021, pp. 792-825.
doi: 10.1177/1475472X211023860

[10] Zwikker, C., and Kosten, C., *Sound Absorbing Materials*, Elsevier, Amsterdam, 1949.

[11] Tijdeman, H., "On the propagation of sound waves in cylindrical tubes," *Journal of Sound and Vibration*, Vol. 39, No. 1, March 1975, pp. 1–33.
[12] Parrott, T., and Jones, M., "Parallel Element Liner Impedances for Improved Absorption of Broadband Sound in Ducts," *Noise Control Engineering Journal*, Vol. 43, No. 6, 1995, pp. 183–195.
[13] Jones, M., Howerton, B., and Ayle, E., "Evaluation of Parallel-Element, Variable-Impedance, Broadband Acoustic Liner Concepts," *AIAA Paper 2012-2194*, 2012.
[14] Coleman T, Branch MA, Grace A. *Optimization toolbox*, vol. 5. For use with MATLAB User's guide for MATLAB, 1999.
[15] Howerton, B. M., Vold, H, and Jones, M. G., "Application of Swept-Sine Excitation for Acoustic Impedance Eduction," AIAA Paper 2019-2487, May 2019.
[16] Jones, M. G., and Stiede, P. E., "Comparison of Methods for Determining Specific Acoustic Impedance," *Journal of the Acoustical Sociey of America*, Vol. 101, No. 5, Pt. 1, pp. 2694-2704, May 1997.
[17] Kreitzman, J and Jones, M. G., "Toward Fully 3D-Printed Two Degree of Freedom Acoustic Liners," Submitted for publication, AIAA SciTech Forum, Jan 2024.